JOURNAL OF MATERIALS SCIENCE 9 (1974) 1536–1544

Review

Thermoplasticity, pseudoelasticity and the memory effects associated with martensitic transformations

Part 2 *The macroscopic mechanical behaviour*

R. V. KRISHNAN,* L. DELAEY, H. TAS†
Departement Metaalkunde, Katholieke Universiteit Leuven, Belgium

H. WARLIMONT
Max-Planck-Institut für Metallforschung, Stuttgart, Germany

The macroscopic mechanical behaviour (stress-strain-temperature relations in tension, compression and internal friction) associated with pseudoelasticity and the memory effects is extensively reviewed. The particular features of the tension and compression curves (the stress to induce or reorient the martensite, total elongation, reversibility and hysteresis) are analysed and their dependence on temperature and crystal orientation is discussed.

1. Introduction

In Part 1 the general characteristics of thermoelasticity, pseudoelasticity and the shape memory effects were discussed. In the present paper experimental evidence on the macroscopic mechanical behaviour is compiled to correlate the various phenomena that are associated with the martensitic transformation. Since the alloys exhibiting pseudoelasticity and shape memory effect possess a high damping capacity related to these effects, this property is also reviewed. The thermoelastic transformation either on cooling or on heating in the absence of an external stress causes no macroscopic mechanical effects. Therefore it will not be considered in the present paper.

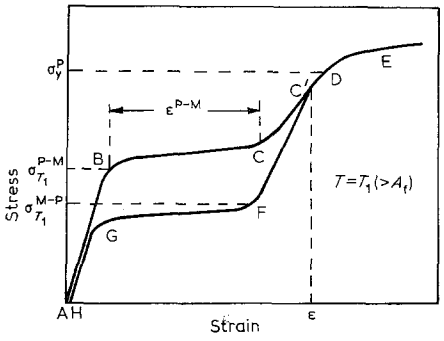

Figure 1 Schematic representation of a stress-strain curve showing the pseudoelastic behaviour. $\rho_T{}^{P-M}$ = stress necessary to cause transformation at T_1; $\rho_T{}^{M-P}$ = stress necessary for reverse transformation at T_1; $\rho_y{}^P$ = plastic yield stress of martensite at T_1; ϵ = total strain achieved; AH = irreversible component of the total strain [2].

2. Pseudoelasticity

2.1. Pseudoelasticity by martensite formation

On stressing a metastable alloy susceptible to transformation to martensite at a constant temperature, T_1, a stress-strain curve as represented in Fig. 1 is obtained, if T_1 is greater than A_f, the temperature at which the reverse transformation is completed under no stress. Section AB represents purely elastic deformation of the parent phase. At point B, corresponding to a stress level $\sigma_{T_1}{}^{P-M}$, the first martensite plates start to form. The transformation is essentially

*Present address: National Aeronautical Laboratory, Bangalore, India
†Present address: Studiecentrum voor Kernenergie (S.C.K.), Mol, Belgium

complete when point C is reached. The slope of section BC reflects the ease with which the transformation proceeds to completion. On continued stressing, the material which is in the completely transformed condition deforms elastically as represented by section CD of the curve. At D, the plastic yield point, σ_p, of the martensite is reached and the material deforms plastically until fracture occurs. If the stress is released before reaching the point D, e.g. at point C′, the strain is recovered in several stages. Part C′F of the curve corresponds to elastic unloading of the martensite. On reaching a stress ${\sigma_T}_1^{M-P}$ at F, the reverse martensitic transformation starts and the fraction of martensite decreases until the parent phase is completely restored (G). Section GH represents the elastic unloading of the parent phase. The total strain may or may not be completely recovered, the latter being the case if some irreversible deformation has taken place either during loading or during unloading. The magnitudes of ${\sigma_T}_1^{P-M}$ and ${\sigma_T}_1^{M-P}$ with respect to the yield stress, σ_y^P, of the parent at T_1 determine the actual tensile behaviour. The difference between ${\sigma_T}_1^{P-M}$ and ${\sigma_T}_1^{M-P}$ determines the stress hysteresis. The area enclosed by the loading and unloading curves gives the amount of the dissipated energy. An experimental stress-strain curve as represented in Fig. 1 was first published by Burkart and Read for indium-thallium alloys in 1953.

The stress necessary to induce the transformation, σ_T^{P-M}, has been found to be a linear function of temperature (Fig. 2). A similar relationship exists for σ_T^{M-P}. The stresses σ_T^{P-M} and σ_T^{M-P} increase with increasing temperature while the yield stress of the β phase, σ_y^P, decreases with increasing temperature, as shown in Fig. 3. The curve shown in Fig. 3 may be divided into three sections: sections AB and A′B″ correspond to stress-strain curves with a large hysteresis; sections BC and B′C′ (which differ in slope from AB and A′B″ respectively) refer to stress-strain curves with a negligible hysteresis and section CD corresponds to the deformation of the parent phase preceding the martensitic transformation.

Further variations of the stress-temperature behaviour shown schematically in Fig. 3 are due to variations of the components of applied stress in relation to the crystal orientation. In their work on In–Tl alloys Burkart and Read [1] found that the slopes of the σ_T^{M-P} and σ_T^{P-M} curves and the hysteresis vary on going from

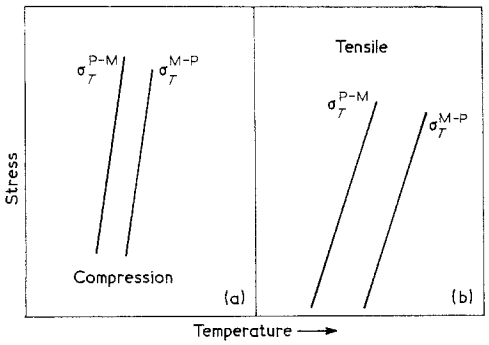

Figure 2 The effect of compressive (a) and tensile (b) loading on martensite formation and disappearance in 20.7% Tl—In alloy [1].

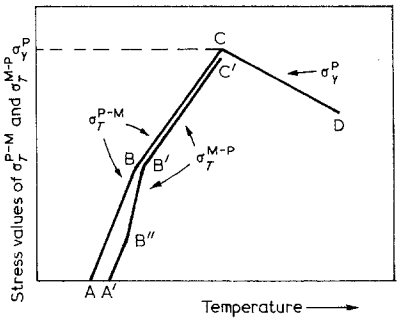

Figure 3 Variation of stress necessary to form martensite with temperature (schematic). Same symbols as in Fig. 1 [3].

tension to compression and on changing the crystal orientation.

Examples of stress-strain curves as a function of testing temperature are given in Figs. 4 and 5. Fig. 4 indicates the striking variation of σ_T^{P-M} and σ_T^{M-P} with testing temperature for Cu–Zn –Si polycrystals. Plotting these stresses against temperature, two straight lines are obtained which intersect the temperature axis ($\sigma = 0$) at M_s and A_s, respectively; these correspond to points A and A′ in Fig. 3. The further features of the σ_T^{P-M} and σ_T^{M-P} behaviour shown schematically in Fig. 3 are illustrated by the stress-strain curves of single crystals of Ag–Cd reproduced in Fig. 5. In Fig. 5a two types of curves can be differentiated regarding the stress hysteresis and the occurrence of serrations. The curves obtained at $T \geqslant 228$ K show nearly no serrations and a small hysteresis whilst those taken at $T \leqslant 218$ K show pronounced serrations and a large hysteresis. A plot of σ_T^{P-M} and σ_T^{M-P} values results in the

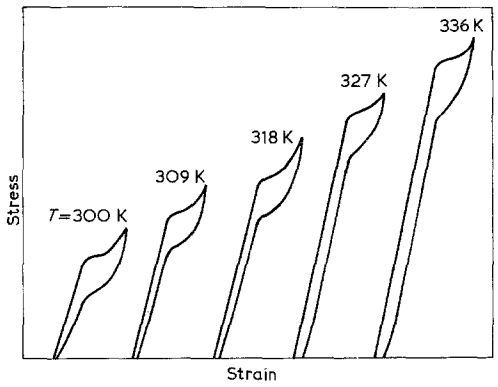

Figure 4 Stress-strain curves showing pseudoelasticity in Cu—Zn—Si alloys as a function of testing temperature [2].

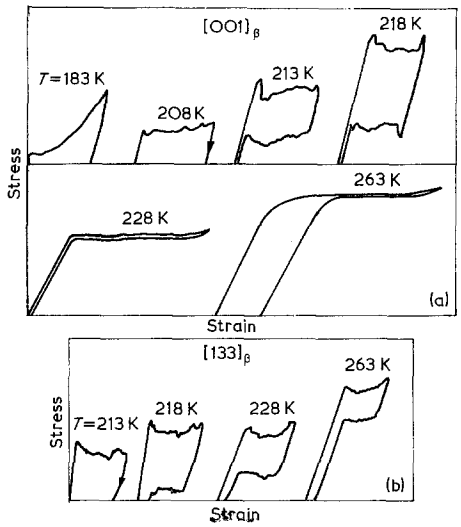

Figure 5 Stress-strain curves showing the pseudoelasticity and shape-memory effect in Ag—45 at. % Cd single crystals as a function of temperature and crystal orientation [3].

temperature dependence shown schematically in Fig. 3.

The martensite plates formed at $T < 228\,K$ grow continuously with increasing stress whereas at $T > 228\,K$ the plates grow spontaneously. In this region nucleation is stress-induced whereas growth is spontaneous, so that a stress relaxation is associated with each growth event. The absence of strain recovery on releasing the applied stress at $T \leqslant 208\,K$ indicates that no reverse transformation occurs in this temperature range. This behaviour is a prerequisite for the memory effect. The incomplete strain recovery at $T = 263\,K$ arises from plastic strain of the matrix prior to martensitic transformation whereas the reverse transformation is complete.

A comparison of Fig. 5a and b indicates that the stress-strain behaviour is a function of the orientation of the tensile axis not only quantitatively but also qualitatively.

The total transformation strain on uniaxial loading, $\epsilon_T{}^{P-M}$, varies from alloy to alloy as a function of the crystallographic parameters. The maximum strains $\epsilon_t{}^{P-M}$ reported from different measurements on single and polycrystalline specimens are given in the third column of Table I. The range of stress at which the maximum transformation strain may be obtained at different temperatures is given in the second column of Table I. The characteristic differences arising with different solvent components will be treated in Part 3. If the values of $\epsilon_t{}^{P-M}$ for single and polycrystalline specimens are compared three main points may be noted.

1. $\sigma_T{}^{P-M}$ is generally lower for polycrystalline material than for single crystal specimens. As mentioned earlier, the stress to initiate the transformation in single crystals is a function of orientation whereas in quasi-isotropic polycrystalline material the most favourable orientation is always present. Therefore the stress for the initiation of transformation in polycrystalline material should correspond to the minimum value for single crystals.

2. The maximum values of $\epsilon_t{}^{P-M}$ for single crystal specimens are given by Fig. 11a to c in Part 1, whilst the maximum strains attainable in polycrystalline specimens of the same alloy will remain lower because of the necessity of accommodation strains at grain boundaries.

3. The residual strain after releasing the stress is higher for the polycrystalline material, implying that the irreversible strain produced by one transformation cycle is higher in this case.

Although tensile or compressive stresses are emphasized as being responsible for pseudoelasticity, the macroscopic behaviour is more clearly revealed on bending. This is caused by the fact that a small linear strain gives rise to a large bending strain in thin specimens.

2.2. Pseudoelasticity by reorientation

On stressing thermal martensite, curves very similar to the ones represented in Fig. 1 are obtained, i.e. pseudoelasticity can also be obtained without being accompanied by a

TABLE I Stress necessary to induce martensite. Transformation strain of pseudoelastic martensite formation

Alloy	σ_T	ϵ_t^{P-M} (max. observed)	specimen remarks s = single crystal p = polycrystal	Strain recovery	Reference
Fe_3Be	47–66 kg mm^{-2}	± 8%	critical resolved shear stress p	± 100%–0 (after several cycles)	13
Ti—51 at. % Ni	50 × 10^{3}psi	± 1, 5%	p	100%	22
Cu—14 wt % Al—3 to 4% Ni	0–40000 psi	± 6%	from −33 to 120°C p	± 100%	4
$AuCd_{47.5}$	9 kg mm^{-2}		at 73°C S	± 100%	23
Cu–Zn–Si Cu–Zn–Sn	0–20.000 psi	15%	0 to 80°C p	± 100%	2
Cu–33%Zn–3wt%Sn	0–30.000 psi	16%	0 to 30°C s + p		17
Ag—Cd (45 at. % Cd)	0–24.000 psi	6%	−70 to 0°C s	± 100%	3

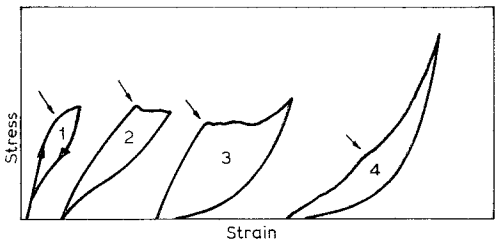

Figure 6 Stress-strain curve of Au—Cd alloys showing pseudoelastic behaviour as a function of the number of cycles [9].

martensitic phase change. This pseudoelasticity is obtained by reorientation. It has been observed in Au–Cd [5], In–Tl [6], Cu–Al–Ni [7], Cu–Al [8] alloys. The stress necessary to initiate the reorientation decreases with increasing number of transformation cycles. This behaviour is shown for an Au–Cd alloy in Fig. 6 [9]. Since the reorientation of the martensite plates can be envisaged as a form of twinning in most cases ([10, 11], see also Part 1), the pseudoelasticity obtained by reorientation can be compared to elastic twinning and untwinning in crystals. Elastic twinning refers to the process of deformation in which a twin, which appears in the crystal upon the application of an external stress, changes its dimensions reversibly with any change in the magnitude of the applied stress. Elastic twinning has been treated extensively by Kosevich and Boiko [12] and by Bolling and Richman [13]. A hysteresis is also observed for elastic twinning; it is considered to arise from a resistive energy similar to that arising from dry friction and from an interfacial energy. Sumino [14] included Au–Cd and In–Tl martensites in his study of the mechanical behaviour of crystals with twinned microstructure. He concluded that the experimental data on these alloys (as in Fig. 6) could not be interpreted in terms of conventional theory of twinning. In fact, the problem is not to consider the nucleation of a twin but rather the motion of existing twin boundaries.

In considering the growth of deformation twins at low stresses, the structural defects of existing twin boundaries have to be taken into account; more specifically, ledges along twin boundaries are highly mobile. Consequently, the stress necessary for twinning along a twin boundary is considerably lower than for twin formation in a bulk crystal. The ratio of the two theoretical shear stresses could be as low as 1/100 in the case of Au–Cd alloy.

The deformation of a martensitic structure capable of reorientation requires a finite applied stress. The process consists essentially of converting martensite of a given variant into a variant of more favourable orientation. It is to be expected that mobile defects exist along the martensite plate boundaries such that an applied stress will give rise to their motion, yielding maximum elongation in the direction of that stress. It has been suggested that the progressing interface sweeps out the existing defects [14]. This possible mechanism along with the activa-

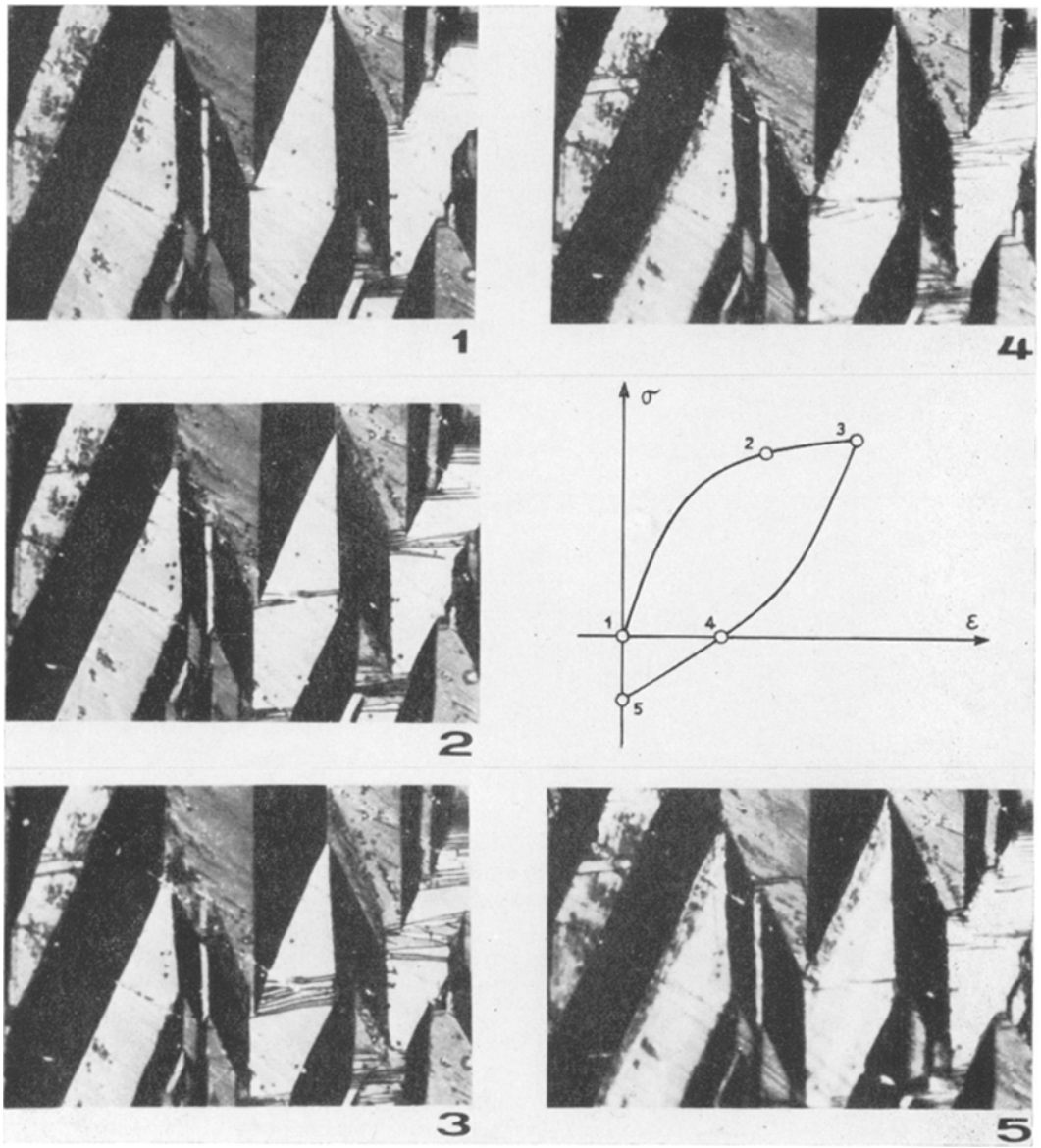

Figure 7 Stress-strain curve and the associated micro-structures of a Cu—Zn—Al—Ni 3R-type of martensite, showing partial pseudoelastic behaviour (1 to 4). 4 and 5 represents the shape recovery (shape memory effect) of the residual strain while heating.

tion of suitably oriented mobile defects in the interfaces during the first loading cycle can explain the decrease in the stress for the onset of reorientation in subsequent cycles.

Other mechanisms for the reorientation of the martensite plates have been proposed by Wasilewski [26]. He concludes that while a suitable stress is applied above M_s the forward austenite-to-martensite transformation can always occur, but that while a stress is applied below A_s only some combinations of stress-and-variant-orientation can lower the start temperature for the reverse transformation, martensite-to-austenite. Therefore the temperature A_d is the equivalent of M_d as determined for a specific transformation variant and not for the onset of the transformation regardless of the variants formed. In his review on the nature of martensitic

DOCKET ALARM

Explore Litigation Insights

Docket Alarm provides insights to develop a more informed litigation strategy and the peace of mind of knowing you're on top of things.

Real-Time Litigation Alerts

Keep your litigation team up-to-date with **real-time alerts** and advanced team management tools built for the enterprise, all while greatly reducing PACER spend.

Our comprehensive service means we can handle Federal, State, and Administrative courts across the country.

Advanced Docket Research

With over 230 million records, Docket Alarm's cloud-native docket research platform finds what other services can't. Coverage includes Federal, State, plus PTAB, TTAB, ITC and NLRB decisions, all in one place.

Identify arguments that have been successful in the past with full text, pinpoint searching. Link to case law cited within any court document via Fastcase.

Analytics At Your Fingertips

Learn what happened the last time a particular judge, opposing counsel or company faced cases similar to yours.

Advanced out-of-the-box PTAB and TTAB analytics are always at your fingertips.

API

Docket Alarm offers a powerful API (application programming interface) to developers that want to integrate case filings into their apps.

LAW FIRMS
Build custom dashboards for your attorneys and clients with live data direct from the court.

Automate many repetitive legal tasks like conflict checks, document management, and marketing.

FINANCIAL INSTITUTIONS
Litigation and bankruptcy checks for companies and debtors.

E-DISCOVERY AND LEGAL VENDORS
Sync your system to PACER to automate legal marketing.